Charge ordering in the rare earth manganates: the experimental situation

2000 J. Phys.: Condens. Matter 12 R83

(http://iopscience.iop.org/0953-8984/12/7/201)

J. Phys.: Condens. Matter **12** (2000) R83–R106. Printed in the UK PII: S0953-8984(00)07533-0

REVIEW ARTICLE

Charge ordering in the rare earth manganates: the experimental situation

C N R Rao†‡‖, Anthony Arulraj†, A K Cheetham‡ and Bernard Raveau§

† Chemistry and Physics of Materials Unit and CSIR Centre of Excellence in Chemistry, Jawaharlal Nehru Centre for Advanced Scientific Research, Jakkur PO, Bangalore 560 064, India
‡ Materials Research Laboratory, University of California, Santa Barbara, CA 93106, USA
§ Laboratorie CRISMAT, ISMRA et Université de Caen, 14050 Caen Cédex, France

E-mail: cnrrao@jncasr.ac.in

Received 26 November 1999

Abstract. Charge-ordered phases of rare earth manganates are novel manifestations arising from interactions between the charge carriers and phonons, giving rise to the localization of carriers at specific sites in the lattice below a certain temperature. Accompanying this phenomenon, the Mn^{3+} (e_g) orbitals and the associated lattice distortions also exhibit long range ordering (orbital ordering). What makes the manganates even more interesting is the occurrence of complex spin ordering related to anisotropic magnetic interactions. In this article, we discuss the emerging scenario of charge-ordered rare earth manganates in the light of specific case studies and highlight some of the new experimental findings related to spin, orbital and charge ordering. We also examine features such as the charge stripes and phase separation found experimentally in these materials, and discuss the factors that affect charge-ordering such as the size of A-site cations and magnetic and electric fields, as well as isotopic and chemical substitutions.

1. Introduction

Charge ordering is a phenomenon observed in solids wherein electrons become localized due to the ordering of cations of differing charges on specific lattice sites. This renders the material insulating. Charge-ordering Fe_3O_4 has been known for some time [1]. The transition from the charge-ordered to the disordered state in Fe_3O_4 at 120 K, identified by Verwey as early as 1939, is associated with a resistivity anomaly. Charge ordering has been found to occur in a few other transition metal oxides as well, but nowhere does it manifest itself as vividly as in rare earth manganates [2]. Accordingly, several of the rare earth manganates of the general composition $Ln_{1-x}A_xMnO_3$ (Ln = rare earth, A = alkaline earth) exhibit fascinating properties and phenomena associated with charge ordering. Historically, the occurrence of charge ordering in these manganates was first observed by Wollan and Koehler [3] and later examined by Jirak *et al* [4]. The situation has since changed significantly due to the discovery of colossal magnetoresistance and other interesting properties in these materials [2, 5].

The rare earth manganates, $Ln_{1-x}A_xMnO_3$, have the perovskite structure just like the parent $LnMnO_3$ compounds, except that the presence of Mn^{4+} ions gives rise to new properties. Thus, while $LaMnO_3$ is an antiferromagnetic insulator with dominant Jahn–Teller effects arising from the presence of the Mn^{3+} ions ($t_{2g}^3e_g^1$), the $Ln_{1-x}A_xMnO_3$ ($x \approx 0.3$) derivatives

‖ Corresponding author.

exhibit ferromagnetism due to double-exchange interaction involving the Mn^{3+}–O–Mn^{4+} units. Since the electrons responsible for electrical conduction in these materials are the same as those responsible for ferromagnetism, they undergo an insulator–metal transition around the Curie temperature, T_C. Magnetic fields reduce the resistivity markedly, particularly around T_C (approaching 100% in favourable instances), giving rise to CMR. The competing interactions in the manganates showing CMR are the Jahn–Teller interaction favouring insulating behaviour and the double exchange favouring the ferromagnetic metallic (FMM) state. Charge ordering also competes with double exchange, and promotes insulating behaviour and antiferromagnetism. Although charge ordering would be expected to be favoured when $x = 0.5$, due to the presence of equal proportions of the Mn^{3+} and Mn^{4+} states, it is found in various compositions in the range $0.3 < x < 0.75$, depending on the Ln and A ions. The charge-ordered phases are novel manifestations arising from the interaction between the charge carriers and the phonons where in the Jahn–Teller distortions play a significant role. Charge ordering arises because the carriers are localized into specific sites below a certain temperature, T_{co}, giving rise to long-range order through out the crystal structure. Furthermore, the Mn^{3+} (e_g) orbitals ($3d_{z^2}$) and the associated lattice distortions (long Mn–O bonds) also develop long-range order, giving rise to orbital ordering. Then, the magnetic exchange interactions between the Mn ions become anisotropic because the Mn–O–Mn superexchange interaction is ferromagnetic through a filled and an empty $3d_{z^2}$ orbital, but antiferromagnetic through two empty $3d_{z^2}$ orbitals. This gives rise to complex magnetic ordering in these structures. Thus, at low temperatures, the rare earth manganates are antiferromagnetically ordered (AFM) with CE or A type ordering, but only the former occurs in the charge-ordered materials where the e_g electrons are localized. The CE-type spin ordering is characterized by the ordering of Mn^{3+} and Mn^{4+} ions alternately. The spin ordering in the *ab* plane is somewhat complex and it stacks antiferromagnetically along the *c* axis. In the A-type spin ordering, the spins order ferromagnetically in the *ab* plane (with the moments pointing towards the *a* axis) and these planes stack antiferromagnetically along the *c* axis. In figure 1 we show the features of CE- and A-type AFM ordering in half-doped manganates ($x = 0.5$). Orbital ordering can occur in both A- and CE-type AFM ordering, but they differ in detail. The CE-type AFM state is attained on cooling a ferromagnetic state or a charge-ordered paramagnetic state.

Investigations of charge ordering in the rare earth manganates in the last three years reveal extraordinary variety in the properties which include their fine sensitivity to the average size of the A-site cations, pressure, magnetic and electrical fields, as well as isotopic and chemical substitutions. The subject is becoming increasingly popular and has to some extent diverted the interest in the rare earth manganates from colossal magnetoresistance to phenomena related to charge ordering. In this article, we shall briefly present the highlights of charge ordering in the rare earth manganates, concentrating on the more recent findings. Adequate presentations of the earlier research in this area up to 1998 can be found in references [2] and [5].

2. Basic features

The basic features of charge-ordering in the perovskite rare earth manganates, $Ln_{1-x}A_xMnO_3$, can be understood by examining the properties of $Pr_{0.6}Ca_{0.4}MnO_3$ and $Nd_{0.5}Sr_{0.5}MnO_3$. These two manganates with different sizes of the A- site cations (the average radius $\langle r_A \rangle$ being 1.17 and 1.24 Å respectively), exhibit significantly different properties. $Pr_{0.6}Ca_{0.4}MnO_3$ is an insulator at all temperatures and becomes charge ordered around 235 K. At this transition temperature, T_{co}, anomalies are found are found in the magnetic susceptibility as well as the resistivity [6] (figure 2). In the charge-ordered (CO) state, the Mn^{3+} and Mn^{4+} ions are regularly arranged in the *ab* plane with the associated ordering of the $d_{x^2-r^2}$ and $d_{y^2-r^2}$ orbitals [7] (figure 3).

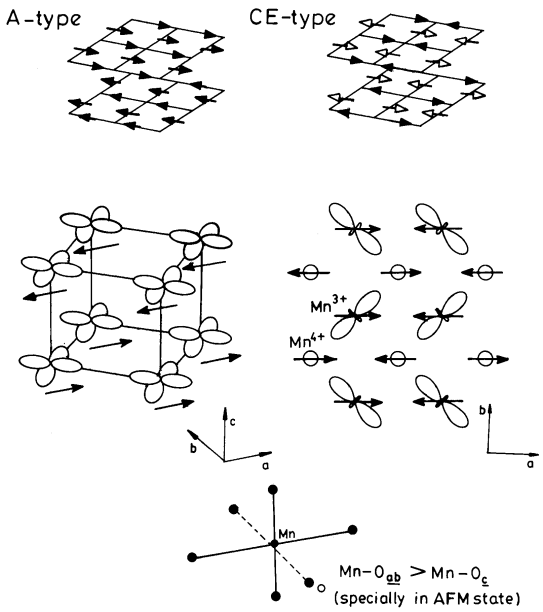

Figure 1. A-type and CE-type antiferromagnetic (AFM) ordering in rare earth manganates, $Ln_{0.5}L_{0.5}MnO_3$. The figure shows spin ordering (*ab* plane) and orbital ordering ($d_{x^2-y^2}$ in A type, $d_{y^2-r^2}$ in CE type) in the two types. The $Mn^{3+}O_6$ octahedra have long Mn–O bonds in the *ab* plane, specially in the AFM state.

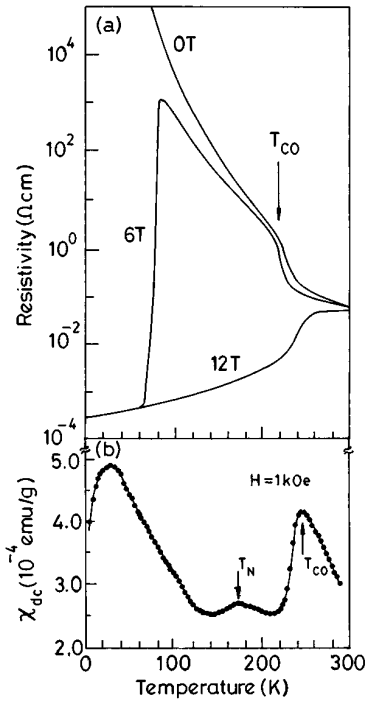

Figure 2. Temperature variation of (a) resistivity and (b) magnetic susceptibility of $Pr_{0.6}Ca_{0.4}MnO_3$ [6].

On cooling, antiferromagnetic (AFM) ordering (CE type) occurs at 170 K (T_N). The CE-type spin structure contains ferromagnetically aligned chains along the *c* axis (figure 3). The ferromagnetic spin ordering in $Pr_{0.6}Ca_{0.4}MnO_3$ is likely to be due to the extra electrons (arising from the deviation from $x = \frac{1}{2}$) which hop in a manner that aligns the t_{2g} spins in the Mn^{4+} sites by the double-exchange mechanism. (It must be noted that $Pr_{0.5}Ca_{0.5}MnO_3$ is a CO material with an antiferromagnetic chain along the *c* axis). Around 40 K, $Pr_{0.6}Ca_{0.4}MnO_3$ exhibits canted antiferromagnetic ordering. Application of an external magnetic field transforms the CO state to a ferromagnetic metallic (FMM) state as shown in figure 2. The transition is first order and is associated with large hysteresis. The magnetic and electrical properties of $Pr_{0.6}Ca_{0.4}MnO_3$ can be represented by the phase diagram [8] in figure 4. The basic features of the CO state in $Pr_{0.6}Ca_{0.4}MnO_3$ are exhibited by other rare earth manganates with relatively small A-size cations, in that the CO state is the ground state. These materials do not become ferromagnetic in the absence of an external field. Thus, $Nd_{0.5}Ca_{0.5}MnO_3$ ($\langle r_A \rangle = 1.17$ Å) is a paramagnetic insulator with a charge-ordering transition around 240 K.

$Nd_{0.5}Sr_{0.5}MnO_3$ is a ferromagnetic metal with a T_C of ∼250 K and transforms to an insulating CO state around 150 K [9] (figure 5). The FMM–CO transition is accompanied by spin and orbital ordering, and the CO insulator is antiferromagnetic (CE type). Application of a

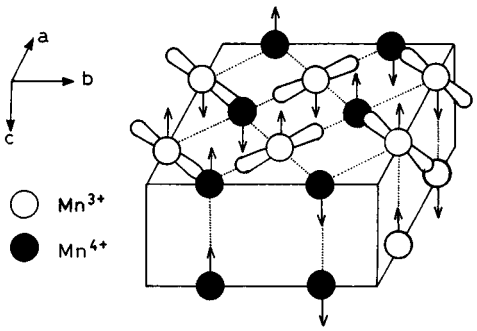

Figure 3. AFM ordering (CE-type) and charge ordering in $Pr_{0.6}Ca_{0.4}MnO_3$. The lobes show the $d_{x^2-r^2}$ or $d_{y^2-r^2}$ orbitals (from Okimoto *et al* [7]).

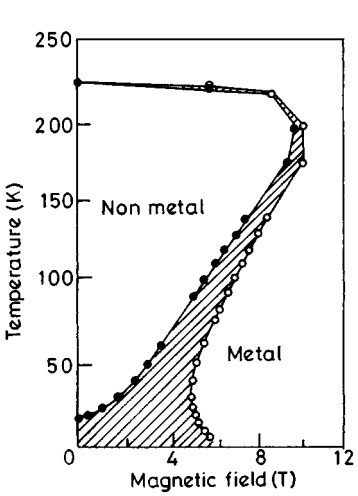

Figure 4. Temperature–magnetic field phase diagram for $Pr_{0.6}Ca_{0.4}MnO_3$ (from Tokura *et al* [8]).

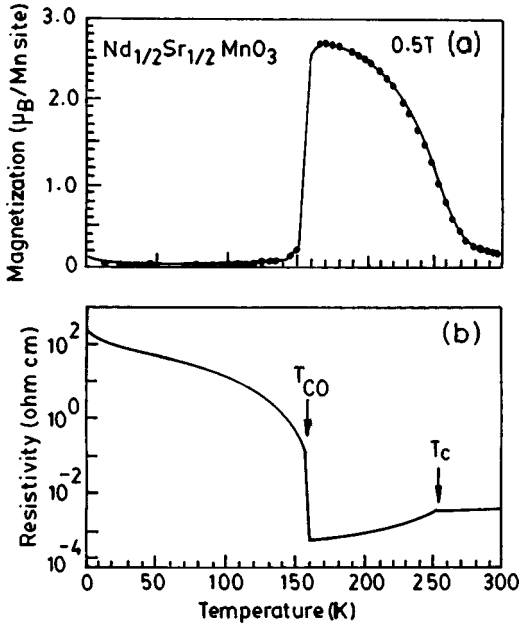

Figure 5. Temperature variation of (a) magnetization and (b) resistivity of $Nd_{0.5}Sr_{0.5}MnO_3$ (from Kuwahara and Tokura [9]).

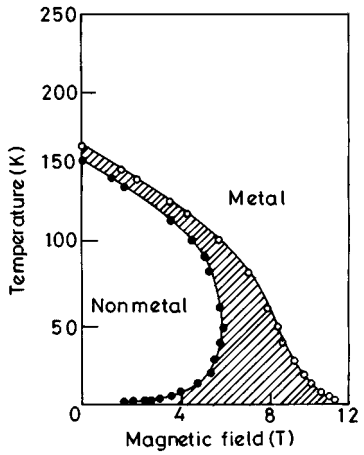

Figure 6. Temperature–magnetic field phase diagram for $Nd_{0.5}Sr_{0.5}MnO_3$ (from Tokura *et al* [8]).

magnetic field of ∼6 T destroys the CO state, and the material becomes metallic. The transition is first order showing hysteresis and is associated with changes in unit cell parameters. The properties of $Nd_{0.5}Sr_{0.5}MnO_3$ can be described in terms of the phase diagram [8] in figure 6. $Pr_{0.5}Sr_{0.5}MnO_3$ undergoes a transition from a FMM state to an AFM state (A type) at 140 K, but is not charge ordered [10]. Note that there can be charge ordering only in the CE-type AFM structure.

We saw that the CO states of both $Nd_{0.5}Sr_{0.5}MnO_3$ and $Pr_{0.6}Ca_{0.4}MnO_3$ could be transformed into the FMM state by the application of magnetic fields. The sensitivity of

the CO state to magnetic fields depends on the average size of the A-site cations, $\langle r_A \rangle$, which in turn determines the Mn–O–Mn angle. We shall discuss this aspect as well as the effects of chemical substitution and other factors on the CO state in later sections. Before doing this, we shall briefly review some of the important recent findings on the CO manganates.

3. Recent results on some manganates

A few decades ago, Goodenough [11] interpreted the CE-type antiferromagnetic structure of $La_{0.5}Ca_{0.5}MnO_3$ as evidence of charge ordering and suggested a possible orbital-ordering pattern associated with it. The crystallographic superstructure arising from such ordering has been observed by electron diffraction and solved by neutron and x-ray diffraction [12]. $La_{0.5}Ca_{0.5}MnO_3$ shows a ferromagnetic transition at 225 K, followed by a first-order transition at 135 K to an AFM (CE) state. The latter transition coincides with a change from incommensurate to nearly commensurate charge ordering. What is surprising, however, is the co-existence of ferromagnetism and charge ordering in the narrow temperature range 220–135 K. This is apparently due to an inhomogeneous spatial mixture of the incommensurate CO and FM (charge-disordered) microdomains [13].

Charge ordering occurs in certain $La_{1-x}Ca_xMnO_3$ compositions with $x > 0.5$ as well. Thus, the $x = \frac{2}{3}$ composition becomes charge ordered around 260 K accompanied by an increase in sound velocity and anomalies in the heat capacity and the activation energy for conduction. In figure 7, we show some characteristics of charge ordering in the $x = 0.63/0.67$ composition [14]. The material becomes antiferromagnetic around 160 K. Transmission electron microscope images of this composition show pairs of $Mn^{3+}O_6$ stripes, with large lattice contractions due to the Jahn–Teller effect, separated by uniform stripes due to the $Mn^{4+}O_6$ octahedra [15]. The periodicities are between two and five times the lattice parameter

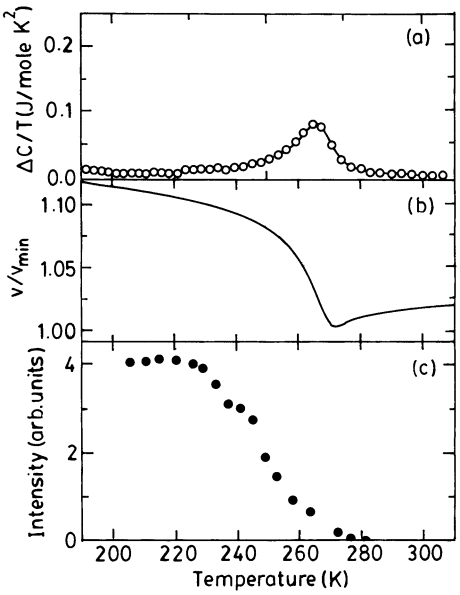

Figure 7. (a) Specific heat divided by temperature, $\Delta C/T$, and (b) sound velocity, v, data for $La_{0.37}Ca_{0.63}MnO_3$; (c) variation of the intensity of the superlattice spots in electron diffraction in $La_{0.33}Ca_{0.67}MnO_3$ (from Ramirez *et al* [14]).

of the orthorhombic unit cell, corresponding to the compositions $x = \frac{1}{2}, \frac{2}{3}, \frac{3}{4}$ and $\frac{4}{5}$ (figure 8). For other values of x, a mixture of the adjacent configurations is seen. Paired Jahn–Teller distorted stripes (JTSs) or bi-stripes are suggested to be the basic building block of the CO state. A structural model for the CO state has been proposed with a unit cell of $3a \times b \times c$, but with the same symmetry as the high temperature state [16]. Although these stripes in electron microscope images have received much attention, it must be noted that these are essentially lattice images. It is not fully clear why the dark contrast arises. One can arrive at a more definitive understanding if high resolution images can be obtained.

The CO and magnetic structures of $La_{0.333}Ca_{0.667}MnO_3$ have been studied in detail [17]. In

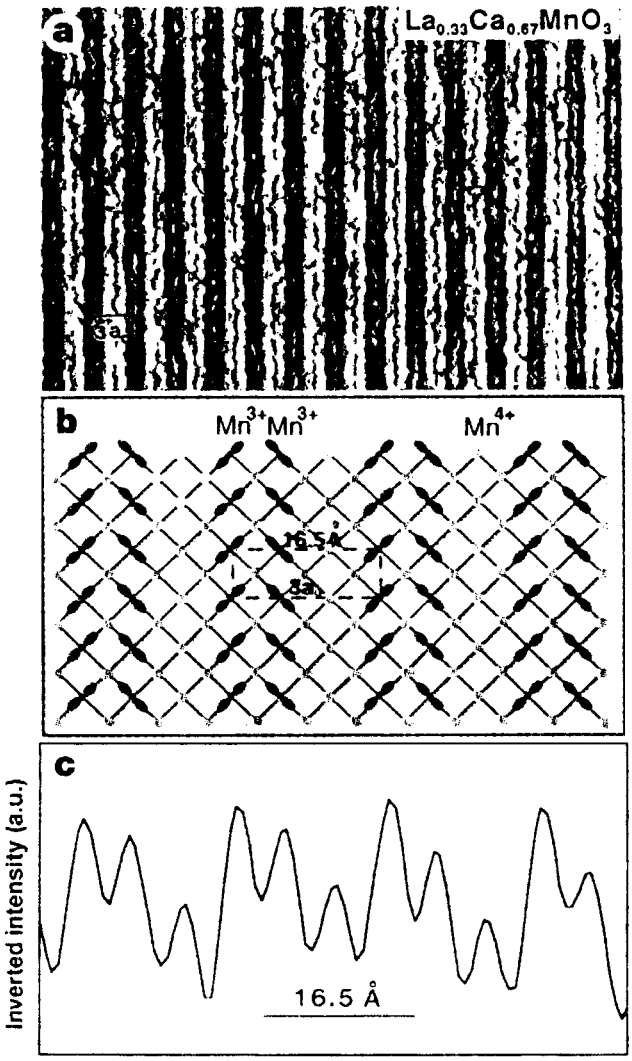

Figure 8. (a) Electron microscope lattice image (95 K) showing $3a$ pairing of $Mn^{3+}O_6$ Jahn–Teller distorted stripes (JTSs) in $La_{0.33}Ca_{0.67}MnO_3$, (b) schematic model in the ab plane showing ordering of JTS (orbitals shown), and Mn^{4+} ions (filled circles), and (c) inverted intensity scan from an area in (a). The pairs of strong peaks are the JTSs (from Mori *et al* [15]).

the AFM structure, the *a* unit cell parameter is tripled and the *c* parameter is doubled relative to the average unit cell. Below T_{co}, the d_{z^2} orbitals of the Jahn–Teller distorted $Mn^{3+}O_6$ octahedra in the *ac* plane of the orthorhombic lattice are ordered (and the *a* parameter is tripled). The Mn^{3+} ions are ordered as far as possible in the *ac* plane and the $Mn^{4+}O_6$ octahedra are displaced in the *c* direction. These features are consistent more with a Wigner-crystal model rather than the bi-stripe pattern (see figure 9) suggested on the basis of transmission electron microscopy [15]. In figure 9, the two models are compared schematically. One possibility is that the electron microscopic data are not representative of the bulk sample. It should be noted that in $La_{0.5}Ca_{0.5}MnO_3$ ($x = \frac{1}{2}$), the bi-stripe and Wigner models are indistinguishable.

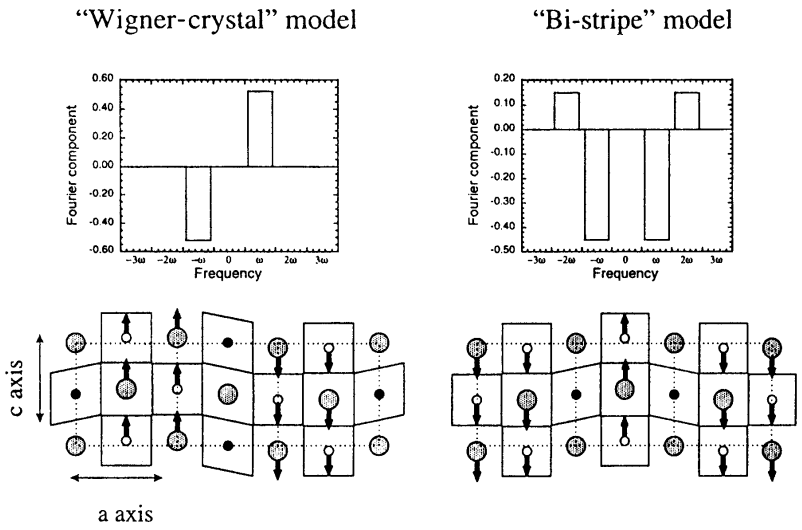

Figure 9. Displacement patterns for the (a) Wigner-crystal and (b) bi-stripe models. Fourier transforms (top) showing the second harmonic component in the bi-stripe model. In the Wigner crystal, a pure sine modulation occurs. Arrows show displacements from the average position of the Mn^{4+} ions (open circles) and of the A-site ion (large shaded circles) (from Radaelli *et al* [17]).

High resolution lattice images of $La_{0.5}Ca_{0.5}MnO_3$ show the CO state to involve a mixture of paired and unpaired Jahn–Teller distorted Mn^{3+} stripes, the unpaired stripes arising from the disordering of the d_{z^2} orbitals concerned [13]. This observation points to the need to distinguish charge ordering and orbital ordering. In the FM phase, charge ordering appears to occur with incommensurate orbital ordering while the FM–AFM transition is associated with an incommensurate to commensurate transition with respect to the orbital degrees of freedom.

Infrared absorption measurements show that the $La_{1-x}Ca_xMnO_3$ samples with $x = 0.5$ and 0.67 both have gaps at a temperature below T_N, providing an explanation for the coexistence of ferromagnetism and charge ordering in the $x = 0.5$ composition [18]. This can be understood if there is separation of the CO and FM phases. Commensurate CO clusters (also AFM) would then compete with the disordered FM domains.

Charge ordering occurs in $Pr_{1-x}Ca_xMnO_3$ in the $0.35 \leqslant x \leqslant 0.5$ composition regime. These compounds show CE-type charge ordering around 230 K (T_{co}) and AFM ordering around 170 K. The paramagnetic state is characterized by ferromagnetic spin fluctuations with a small energy scale [19]. At T_{co}, these fluctuations decrease and disappear at T_N. Electron diffraction and dark-field TEM images show the presence of incommensurate charge ordering in the paramagnetic insulating state (180–260 K) of the $x = 0.5$ composition [20]. At T_N, there is an incommensurate–commensurate CO transition. In the incommensurate CO structure, partial

orbital ordering is likely to be present. Similar charge, orbital and spin ordering has been found in the 0.3 composition as well [21]. Optical conductivity spectra of the $x = 0.4$ composition show evidence of spatial charge and orbital ordering at 10 K [7]. The CO state has a gap of $\sim$0.2 eV which is transformed into a metallic state on applying a magnetic field (6 T), the gap appearing up to 4.5 T. The gap value is the order parameter of the CO state and couples with spin ordering.

$Pr_{0.67}Ca_{0.33}MnO_3$ shows thermal relaxation effects from the metastable FMM state (produced by the application of a 10 T magnetic field) to the CO state [22]. The metal–insulator transition is observed as an abrupt jump in resistivity at a well defined time, depending on the temperature. This observation indicates the percolative nature of current transport. A recent electron microscopic study of $La_{1-x-y}Pr_yCa_xMnO_3$ with $x = 3/8$ has shown that this manganate is electronically phase separated into a sub-micrometre-scale mixture of CO insulating regions and metallic, ferromagnetic domains [23] (figure 10). The balance between the two states is affected by changes in chemical substitution, magnetic field etc. Percolative transport between the two states could be responsible for the high CMR in such manganates with low T_C.

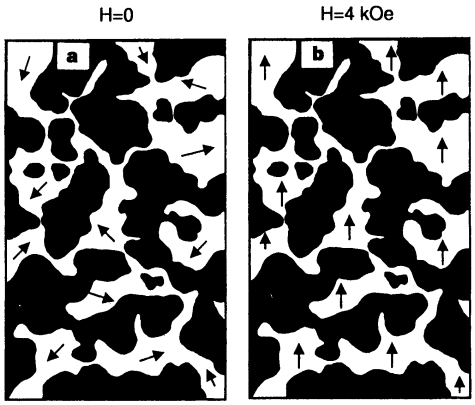

Figure 10. Schematic diagram showing the co-existence of CO insulating phase (dark area) and FMM (white area) domains in $La_{1-x-y}Pr_yCa_xMnO_3$. The domain sizes are $\sim$0.5 μm. Magnetization directions (arrows) show alignment in a magnetic field (b), and randomness in (a) (from Uehara *et al* [23]).

The first-order transition of $Nd_{0.5}Sr_{0.5}MnO_3$ from the FMM state to the CO-AFM state has been well documented [24]. The *Imma* space group of this manganate renders the Mn–O–Mn angle in the *ab* plane closer to 180°, promoting the overlap of the Mn(e_g) and O(2p) orbitals. The e_g electrons are delocalized in the FMM state, but localized in the AFM (CE) state below T_{co}. In the A-type AFM state found in the $x > 0.5$ composition, however, the e_g electrons are delocalized in the *ab* plane. Vacuum tunnelling measurements show that at the 150 K transition, a CO gap of 250 meV opens up [25]. Photoemission studies indicate a sudden change in electron states at the transition and give an estimate of 100 meV for the gap [26]. These estimates of the gap are considerably larger than T_{co} (12 meV) and it is not clear how a magnetic field of 6 T (1.2 meV) destroys the CO state. Recent tunnelling studies show that the gap collapses on applying the magnetic field, suggesting that a gap in the density of states at E_F is necessary for the stability of the CO state [27].

$Nd_{0.5}Sr_{0.5}MnO_3$ shows anomalous magnetostriction behaviour, with a large positive magneto-volume effect as shown in figure 11, due to the magnetic field induced structural

transition accompanying the CO–FMM transition [28]. It is to be noted that the unit cell volume of the FMM phase is higher than that of the CO phase. In $Pr_{0.7}Ca_{0.3}MnO_3$, the destruction of the CO state gives rise to a negative magneto-volume effect. It appears that the magnetic field induced structural transition occurs when the CO state is established in the FM state, as in $Nd_{0.5}Sr_{0.5}MnO_3$. The magneto-volume effect in $Nd_{0.5}Sr_{0.5}MnO_3$ is consistent with the existence of an electron phase segregation at low temperatures which is reversed by a magnetic field. Magnetization and other measurements suggest the presence of FM domains in the CO state at low temperatures [28].

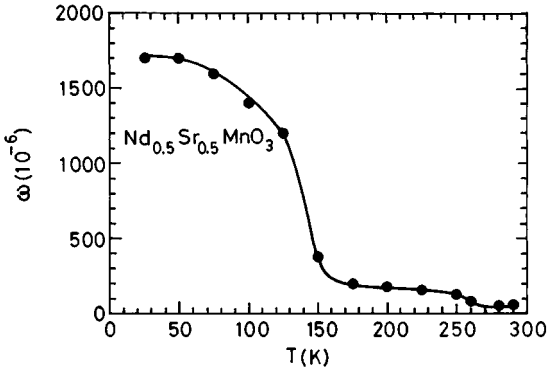

Figure 11. Temperature variation of the maximum volume magnetostriction in $Nd_{0.5}Sr_{0.5}MnO_3$ at 13.7 T (from Mahendiran *et al* [28]).

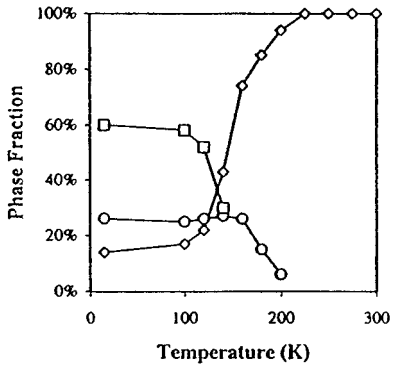

Figure 12. Variation in the percentage of the different phases of $Nd_{0.5}Sr_{0.5}MnO_3$ with temperature: FMM phase (diamonds); orbitally ordered A-type AFM phase (squares); charge-ordered CE-type AFM phase (circles) (from Woodward *et al* [29]).

High resolution x-ray and neutron diffraction investigations show that $Nd_{0.5}Sr_{0.5}MnO_3$ phase separates into three macroscopic phases at low temperatures. These are the FMM high temperature phase ($Imma$), the orbitally ordered AFM (A-type) phase ($Imma$) and the charge- and orbitally ordered AFM (CE-type) low temperature phase ($P2_1/m$) [29]. The A-type AFM phase starts manifesting itself around 220 K, while the CE-type CO phase first appears at 150 K. In figure 12, we show the phase compositions at different temperatures. The presence of the high temperature FMM phase, even at very low temperatures, is noteworthy. These results are of considerable significance in interpreting many properties of this manganate. The FMM phase has a larger volume than the average volume or the volume of the low temperature CO

phase. A reasonably satisfactory magnetic phase diagram of $Nd_{1-x}Sr_xMnO_3$ is available [30]. The phase segregation behaviour of this system and the relative stabilities of the structures seem to depend crucially on the Mn^{4+}/Mn^{3+} ratio. Thus, $Mn^{4+}/Mn^{3+} > 1$ appears to stabilize the orbitally ordered AFM (A-type) phase [29]. Unlike $Nd_{0.5}Sr_{0.5}MnO_3$, $Nd_{0.45}Sr_{0.55}MnO_3$ has an A-type AFM state below T_N (220 K) and metallicity is confined to the ferromagnetic *ab* plane below T_N while along the *c*-axis it is insulating (figure 13). The large anisotropy in this material implies that the carriers are confined to the ferromagnetic layer, by magnetic and orbital ordering [31].

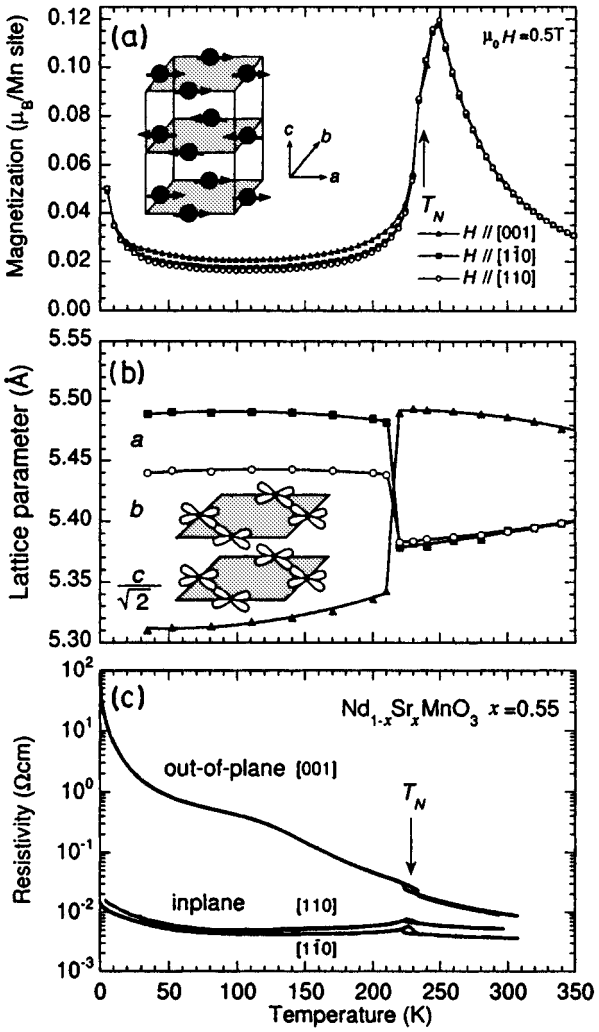

Figure 13. Temperature variation of (a) magnetization, (b) lattice parameters and (c) resistivity of $Nd_{0.45}Sr_{0.55}MnO_3$. Spin ordering and orbital ($d_x^2 - d_y^2$) ordering in this A-type AFM material are shown in (a) and (b) respectively (from Kuwahara *et al* [31]).

$Ca_{1-x}Bi_xMnO_3$ ($0.0 < x \leqslant 0.3$) shows charge ordering, the transition temperature depending on x, with a T_{co} of ∼300 K for $x = 0.3$ [32]. There are ferromagnetic correlations in the paramagnetic regime ($T > T_{co}$) and antiferromagnetic ordering occurs

at low temperatures. Below T_N, a CO gap develops, but in the $T_N < T < T_{co}$ regime, FM and AFM domains seem to coexist, indicating phase separation [33]. Charge stripes resulting from charge ordering are observed around T_{co} in $Ca_{0.76}Bi_{0.24}MnO_3$, demonstrating the strong interaction between the charge and the lattice [34]. Such a coupling would be expected to change the Mn–O bond length. Electron energy loss spectroscopic measurements indeed show that hybridization between the oxygen (2p) and Mn (3d) orbitals is weakened due to the lattice distortion caused by charge ordering [35]. Manganates of the type $Ca_{1-x}Bi_xMnO_3$ or $Ca_{1-x}Ln_xMnO_3$ ($x < 0.5$) have been considered to be electron doped, rather than hole doped as in $Ln_{1-x}A_xMnO_3$ ($x < 0.5$) [32, 36]. Thus, $La_{0.333}Ca_{0.667}MnO_3$ discussed earlier is electron doped. A noteworthy feature of the electron doped materials is the increase in T_{co} with increase in the electron concentration or x. What is noteworthy, however, is that the electron-doped manganates do not generally exhibit ferromagnetism. Clearly, there is electron–hole asymmetry in these manganates.

4. Effect of the size of the A-site cations

In the manganates exhibiting CMR, the ferromagnetic T_C increases with the average radius of the A-site cations, $\langle r_A \rangle$. Increasing $\langle r_A \rangle$, which is equivalent to increasing the hydrostatic pressure, increases the Mn–O–Mn angle and e_g bandwidth. If there is considerable mismatch in the radii of the different A-site cations, however, T_C does not increase with $\langle r_A \rangle$, an aspect that we will discuss later. The charge-ordering transition is also highly sensitive to $\langle r_A \rangle$ and T_{co} increases with decrease in $\langle r_A \rangle$. The sensitivity of T_{co} to $\langle r_A \rangle$ has been discussed in some detail recently [2, 37, 38] and is generally attributed to an increased tilting of the MnO_6 octahedra as $\langle r_A \rangle$ decreases. Infrared absorption spectra show prominent band splittings (and increase in phonon frequencies) at $T \leqslant T_{co}$, indicative of octahedral distortions [39]. In figure 14, we show the phase diagrams [37] of $Ln_{0.5}Sr_{0.5}MnO_3$ and $La_{0.5}Ca_{0.5}MnO_3$ to illustrate some of the important features. Careful structural investigations [37] show that the Mn–O(eq)–Mn and Mn–O(ax)–Mn bonds are identical in $La_{0.5}Ca_{0.5}MnO_3$ (expect when Ln = La). For $Ln_{0.5}Ca_{0.5}MnO_3$ and all the $Ln_{0.5}Sr_{0.5}MnO_3$ compounds, the Mn–O(eq)–Mn angle is significantly larger (2–6°) than the Mn–O(ax)–Mn angle. While the $La_{0.5}Ca_{0.5}MnO_3$ manganates crystallize in *Pnma* symmetry, in the $Ln_{0.5}Sr_{0.5}MnO_3$ manganates, there is an evolution from *Pnma* to $I4/mcm$ through *Imma* with increase in $\langle r_A \rangle$. The changes in the octahedral tilt system have consequences for the low temperature magnetic structure. This is seen in $Nd_{0.5}Sr_{0.5}MnO_3$ where the charge ordering in the CE-type AFM state is associated with the *Imma* structure.

It was mentioned earlier that the CO states of $Nd_{0.5}Sr_{0.5}MnO_3$ ($\langle r_A \rangle = 1.24$ Å) and $Pr_{0.6}Ca_{0.4}MnO_4$ ($\langle r_A \rangle = 1.17$ Å) are both destroyed by magnetic fields. The field required to melt the CO state varies with $\langle r_A \rangle$ and the manganates with very small $\langle r_A \rangle$ remain charge ordered even on application of high magnetic fields [2, 38]. Thus, $Y_{0.5}Ca_{0.5}MnO_3$ ($\langle r_A \rangle = 1.13$ Å) has a very robust CO state which is not affected by high magnetic fields (> 15 T). We can thus distinguish three types of manganate with respect to their sensitivity to magnetic fields [38]: (a) manganates that are ferromagnetic and become charge ordered at low temperatures (e.g., $Nd_{0.5}Sr_{0.5}MnO_3$), with the CO state transforming to an FMM state on application of a magnetic field, (b) manganates that are charge ordered in the paramagnetic state and do not exhibit an FMM state, but transform to an FMM state under a magnetic field (e.g. $Pr_{1-x}Ca_xMnO_3$) and (c) those which are charge ordered in the paramagnetic state as in (b), but are not affected by magnetic fields up to ~5 T (e.g. $Y_{0.5}Ca_{0.5}MnO_3$). Some of the manganates in category (c), such as $Nd_{0.5}Ca_{0.5}MnO_3$, show a CO → metal transition only on the application of very high fields (⩾15 T). The $x = 0.5$ manganates with $\langle r_A \rangle = 1.17$ Å seem to belong to

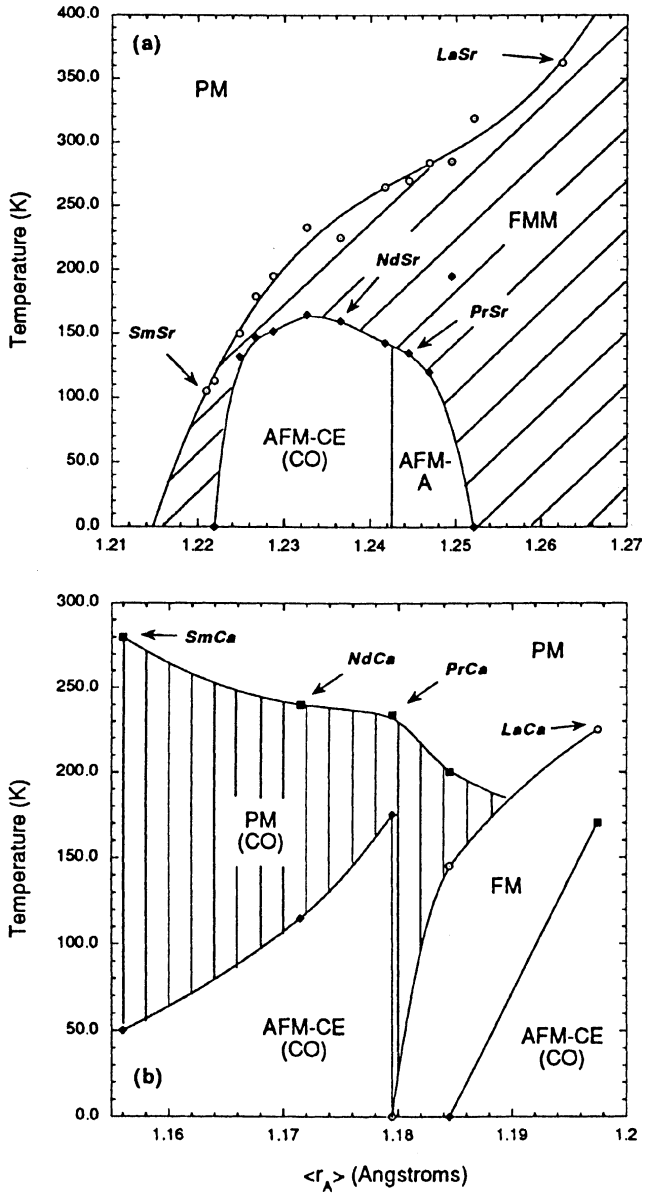

Figure 14. Temperature–$\langle r_A \rangle$ phase diagrams for (a) $Ln_{0.5}Sr_{0.5}MnO_3$ and (b) $La_{0.5}Ca_{0.5}MnO_3$ (from Woodward *et al* [37]).

category (c). The apparent one-electron bandwidths estimated on the basis of the experimental Mn–O–Mn angles and Mn–O distances in $Ln_{0.5}L_{0.5}MnO_3$ do not vary significantly with $\langle r_A \rangle$, suggesting that other factors may be responsible for the sensitivity of the CO state to $\langle r_A \rangle$. One possibility is the competition between A- and B-site cations for covalent mixing with the O(2p) orbitals [38]. In the so-called electron-doped manganates, $Ca_{1-x}Ln_xMnO_3$ and $Ca_{1-x}Bi_xMnO_3$ ($x < 0.5$), T_{co} is found to decrease with the decrease in $\langle r_A \rangle$ [32]. Furthermore, T_{co} increases with electron concentration or x. These features distinguish electron-doped

manganates from the $Ln_{1-x}A_xMnO_3$ ($x = 0.5$) series of manganates.

By increasing the size of the A-site cations, the CO state in manganates can be transformed to an FMM state [40]. Here also, increasing $\langle r_A \rangle$ has the same effect as increasing the external pressure [41]. In figure 15, we show the effect of internal pressure on the CO state of $Pr_{0.7}Ca_{0.3}MnO_3$ wherein Ca is substituted by the larger Sr or Pr is substituted by La. In the $Pr_{0.5}Sr_{0.5-x}Ca_xMnO_3$ system [42], T_C decreases with increase in x or decrease in $\langle r_A \rangle$ up to $x = 0.25$; $T_{co} = T_N$ from $x = 0.09$ to 0.25. When $\langle r_A \rangle$ is further decreased, T_{co} increases from 180 K for $x = 0.25$ to 250 K for $x = 0.30$; for $0.30 \leqslant x \leqslant 0.50$, $T_{co} > T_N$. In $Pr_{0.6}(Ca_{1-x}Sr_x)_{0.4}MnO_3$, charge ordering is removed for $x > 0.15$ and the material becomes ferromagnetic [43]. Specific heat measurements show that when $x > 0.25$, the materials are

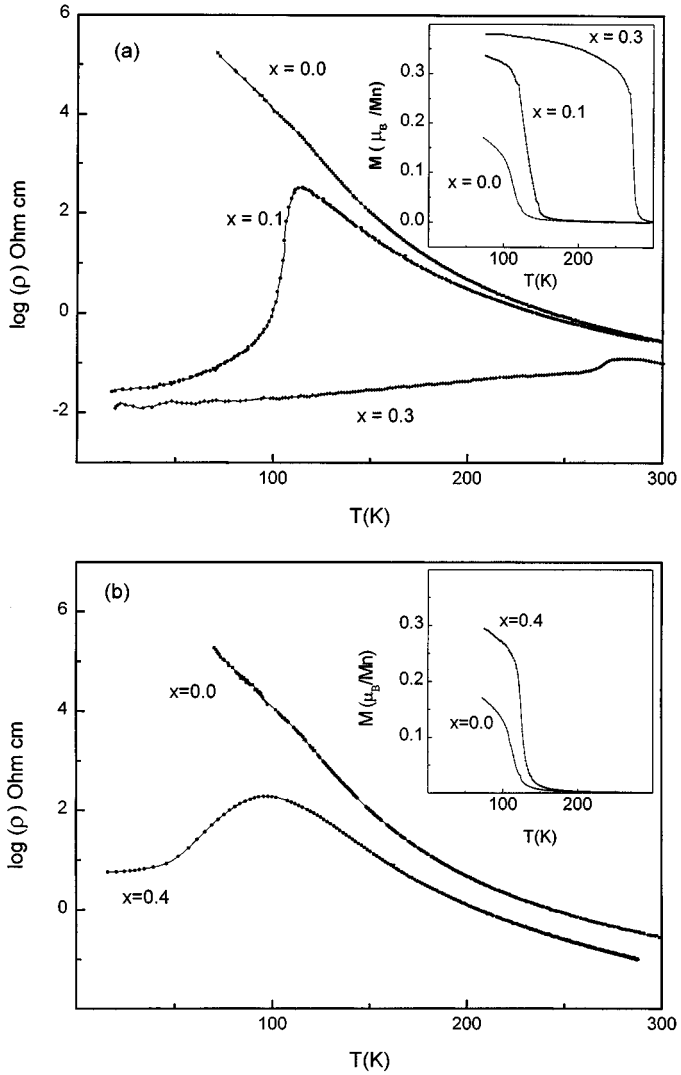

Figure 15. Effect of internal pressure on the properties of (a) $Pr_{0.7}Ca_{0.3-x}Sr_xMnO_3$ and (b) $Pr_{0.7-x}La_xCa_{0.3}MnO_3$. Note that substitution by a larger A-site cation renders the material ferromagnetic (see insets). An insulator–metal transition is also observed (from Rao *et al* [40]).

ferromagnetic with small γ values; when $x \leqslant 0.25$, they are charge ordered with contributions from magnetic ordering [44].

The effect of cation size disorder on the ferromagnetic T_C of rare earth manganates exhibiting CMR has been investigated in detail [36, 45, 46]. In these studies, T_C has been related to the variance in the distribution of $\langle r_A \rangle$, as defined by Attfield [47]. The ferromagnetic T_C decreases significantly with the variance, σ^2, based on the studies of manganates with fixed $\langle r_A \rangle$. A similar study of the variation of T_{co} with σ^2 in $Ln_{0.5}A_{0.5}MnO_3$ for fixed $\langle r_A \rangle$ values of 1.17 and 1.24 Å, has shown that T_{co} is not very sensitive to the size mismatch [48]. In figure 16, we show the variation of T_{co} with σ^2 to illustrate this feature. It would appear that the Jahn–Teller effect and Coulomb interactions play a more important role in determining the nature of the CO state in these materials.

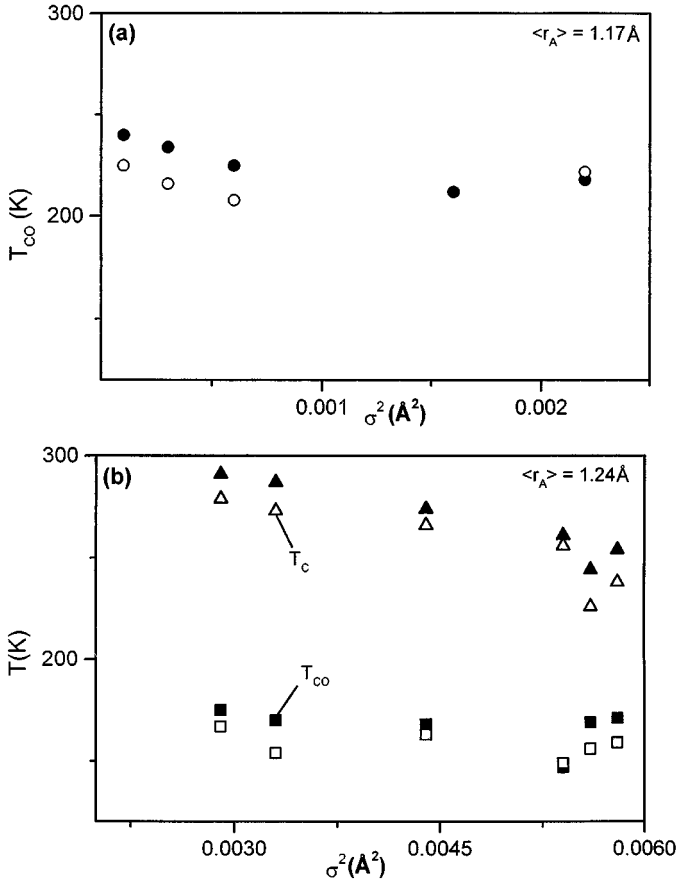

Figure 16. Variation of the charge-ordering transition temperature with σ^2 for fixed $\langle r_A \rangle$ of (a) 1.17 Å and (b) 1.24 Å. In the latter case, variation of T_C is also shown. Note that T_C decreases markedly with increase in σ^2 unlike T_{co} (from Vanitha *et al* [48]). Filled symbols are from magnetic measurements and open symbols from resistivity measurements.

While one employs $\langle r_A \rangle$ as a parameter to vary the e_g bandwidth for convenience, it should be realized that there are no simple systematics in charge-ordering and magnetic behaviour of $Ln_{0.5}L_{0.5}MnO_3$ compounds with $\langle r_A \rangle$. Considering that the rare earth manganates with large $\langle r_A \rangle$, as exemplified by $Nd_{0.5}Sr_{0.5}MnO_3$ ($\langle r_A \rangle = 1.24$ Å), and those with small $\langle r_A \rangle$, as

exemplified by $Nd_{0.5}Ca_{0.5}MnO_3$ ($\langle r_A \rangle = 1.17$ Å), exhibit entirely different characteristics of the CO state, and that $\langle r_A \rangle = 1.17$ Å categorizes the manganates with respect to the effect of the magnetic fields, we would expect interesting and unusual properties in the intermediate range of $\langle r_A \rangle$ of 1.20 ± 0.20 Å. In this regime T_{co} approaches T_C leading to a competition between charge ordering and ferromagnetism. Thus, $La_{0.5}Ca_{0.5}MnO_3$ ($\langle r_A \rangle = 1.20$ Å) exhibits a region of coexistence of ferromagnetism and charge ordering as discussed earlier. In $(Nd_{1-x}Sm_x)_{0.5}Sr_{0.5}MnO_3$, T_C decreases from 255 to 115 K as x increases from 0.0 to 0.875, as expected for a decrease in $\langle r_A \rangle$ [49]. Surprisingly, T_{co} also decreases from 158 to 0 K as x changes from 0.0 to 0.875. This unusual behaviour wherein T_{co} is suppressed as T_C approaches T_{co} is interesting. It is to be noted that the variance due to size mismatch, σ^2, does not vary significantly with x in this system, the range being 0.005–0.008. This would also decrease the T_{co}.

$Nd_{0.25}La_{0.25}Ca_{0.5}MnO_3$ ($\langle r_A \rangle = 1.19$ Å) reveals an intriguing sequence of phase transitions [50]. On cooling, this manganate develops an incipient CO state below 220 K. The formation of this state is accompanied by an increase in electrical resistivity and the opening up of a gap in the density of states near E_F. The orthorhombic distortion also increases, as a consequence of cooperative Jahn–Teller distortion of the lattice and short range ordering of the Mn^{3+} and Mn^{4+} ions. Around 150 K, the incipient CO state becomes unstable and the material undergoes a re-entrant transition to an FMM state. The transition is characterized by a sharp decrease in resistivity, collapse of the CO gap, development of FM ordering and an abrupt decrease in the orthorhombic distortion. There is a two phase coexistence region (150–220 K) around the CO–FMM transition.

5. Layered manganates

The unique interplay of spin, orbital and charge ordering in the rare earth manganates in determining their properties has been evident from the earlier discussion of the perovskite manganates. These factors become even clearer from a study of the layered manganates. In the Ruddlesden–Popper manganates, $(Ln, A)_{n+1}Mn_nO_{3n+1}$, the $n = \infty$ phase is the perovskite, $Ln_{1-x}A_xMnO_3$. The $n = 2$ phases, such as $La_{2-x2x}Sr_{1+2x}Mn_2O_7$, show a metallic ground state for $x \geqslant 0.17$ and high CMR, besides exhibiting many interesting properties arising from the layered nature of the materials. The $n = 1$ member, $Ln_{1-x}Sr_{1+x}MnO_4$, however, does not become metallic up to $x = 0.7$. $La_{0.5}Sr_{1.5}MnO_4$ shows ordering of the Mn^{3+} and Mn^{4+} ions around 220 K, accompanied by the ordering of the e_g orbitals (figure 17), and the material becomes antiferromagnetic at 110 K. Anisotropic properties arising from orbital ordering in this manganate have been investigated [51]. During the 220 K transition, there is a significant change in the conductivity spectrum. The order parameter for orbital ordering increases at T_{co}, grows further with decrease in temperature and decreases on spin ordering at T_N. The order parameter for charge ordering appears to evolve along with that due to orbital ordering. Application of high magnetic fields causes metamagnetic transitions below T_{co}; both charge and orbital orderings are destroyed by the magnetic field [52]. Thermal conductivity measurements show the prevalence of stripe correlations [53], just as in $Ln_{1.67}Sr_{0.3}NiO_4$. $Nd_{0.5}Sr_{1.5}MnO_4$ and other rare earth analogues do not show charge ordering.

Charge ordering in $LaSr_2Mn_2O_7$ ($n = 2$) has been identified by electron diffraction [54]. A recent Raman study [55] has shown that dynamic charge-ordering correlations occur in the 16–340 K range, becoming static over a narrow range below T_{co} (210 K). Superlattice reflections are found in the static regime. The degree of charge and orbital ordering in this manganate is suspected to be weaker than in the three- dimensional perovskites. There is need for a detailed study of charge ordering in this manganate as well as in other rare earth derivatives, including the calcium analogues.

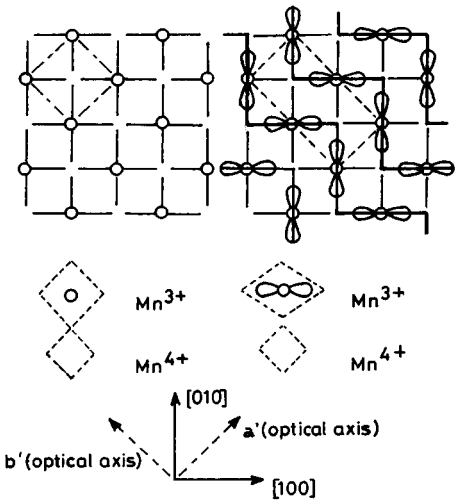

Figure 17. (a) Charge ordering in $La_{0.5}Sr_{1.5}MnO_4$ with a schematic representation of the oxide ion displacements; (b) schematic representation of the oxide ion displacements. Mn^{3+} (e_g) orbitals are shown (from Ishikawa *et al* [51]).

6. Effect of substitution in the Mn site

Substitution of Mn by cations such as Al^{3+} and Fe^{3+} in charge-ordered manganates does not have an immediate effect, but charge ordering is destroyed at moderate doping ($x \gtrsim 0.03$). However, substitution by Cr^{3+} and Co^{3+} destroys charge ordering readily and renders the material ferromagnetic and metallic; in this respect, Cr^{3+} is specially effective [2, 36, 56]. In $Sm_{0.5}Ca_{0.5}Mn_{1-x}Cr_xO_3$, the T_{co} (275 K when $x = 0.0$) decreases with increase in x and charge ordering disappears at $x = 0.05$. The $x = 0.05$ composition shows a insulator–metal transition when the material becomes ferromagnetic [57]. The effectiveness of Cr^{3+} in destroying the CO state was considered to be due to its favourable electronic configuration (t_{2g}^3), which is the same as that of Mn^{4+}. However, Cr^{3+} in the Mn^{3+} site would be immediately surrounded by Mn^{4+} ions which would not allow electron hopping. It would be more favourable if Mn^{4+} were substituted by an appropriate quadrivalent cation such as Ru^{4+} ($t_{29}^4 e_g^0$). Recent studies [56] have shown that substitution of Mn by Ru in $Nd_{0.5}Ca_{0.5}MnO_3$ destroys charge ordering and renders this material ferromagnetic with the T_C increasing with Ru content; the material also shows a insulator–metal transition (figure 18). The marked effect of Ru substitution is also seen in $Nd_{0.5}Sr_{0.5}MnO_3$ where T_C increases with the Ru content to well above 300 K, while the charge ordering is destroyed (figure 19).

7. Oxygen isotope effect

Substitution of ^{16}O by ^{18}O has a marked effect on the magnetic properties and CMR of the manganates, indicating the important role of electron–phonon coupling. Substituting ^{18}O for ^{16}O in $La_{0.175}Pr_{0.52}Ca_{0.3}MnO_3$ destroys the insulator–metal transition and renders the material insulating down to 4 K [58]. The charge-ordering transition in $La_{0.5}Ca_{0.5}MnO_3$ increases by 9 K upon replacing ^{16}O by ^{18}O; the isotope shift increases with the magnetic field in $La_{0.5}Ca_{0.5}MnO_3$ as well as in $Nd_{0.5}Sr_{0.5}MnO_3$ [59]. In $Pr_{0.67}Ca_{0.33}MnO_3$, the magnetic field induced insulator–metal transition occurs at a higher field on ^{18}O substitution; the heavier

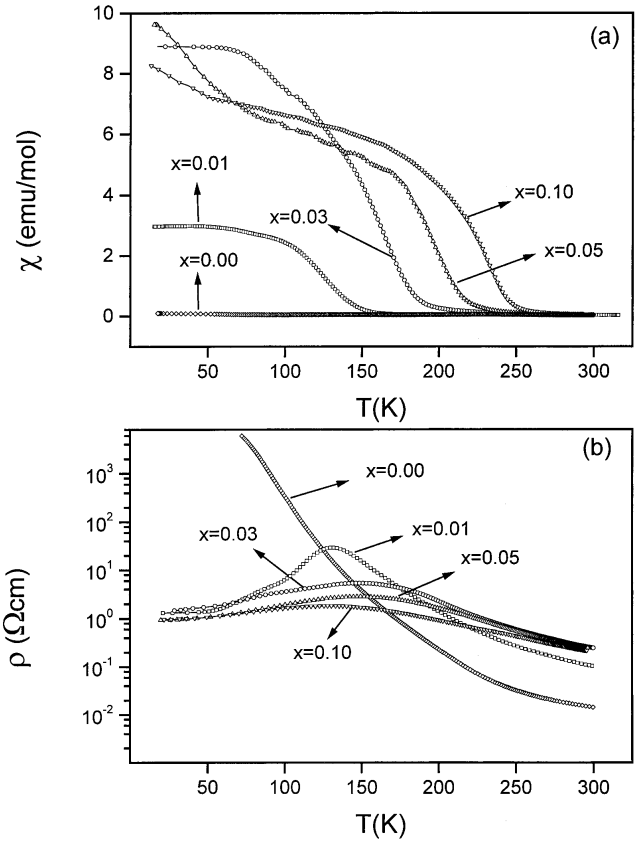

Figure 18. Temperature variation of the (a) magnetic susceptibility and (b) resistivity of $Nd_{0.5}Ca_{0.5}Mn_{1-x}Ru_xO_4$ (from Vanitha *et al* [56]).

isotope favours the insulating state [60]. The isotope effect on T_{co} is greater in $Nd_{0.5}Sr_{0.5}MnO_4$ than $Pr_{0.5}Ca_{0.5}MnO_3$, showing the role of $\langle r_A \rangle$ as well [61].

8. Effect of electric fields and related aspects

The effect of magnetic fields on the CO states of rare earth manganates was discussed earlier. In $Pr_{1-x}Ca_xMnO_3$ ($x \approx 0.4$), magnetic fields cause a CO–FMM transition. High electric fields and x-irradiation also give rise to such a transition. Irradiation with visible light at small electric fields is reported to delocalize the CO state, causing an insulator–metal transition [62]. The light induced insulator–metal transition in $Pr_{0.7}Ca_{0.3}MnO_3$ appears to generate a localized conduction path, although the bulk of the sample is insulating [63]. X-ray irradiation causes photo-induced structural change, accompanied by the destruction of the CO state in $La_{0.875}Sr_{0.125}MnO_3$ [64].

A recent study of the electric field induced effects in thin films of several charge-ordered rare earth manganates including $Nd_{0.5}Ca_{0.5}MnO_3$ and $Pr_{0.7}Ca_{0.3}MnO_3$ shows that very small dc currents (fields) destroy the CO state and give rise to insulator–metal transitions [65]. The current–voltage characteristics are non-ohmic and show hysteresis. The I–M transition temperature decreases with increasing current (figure 20). The hysteretic I–M transition in

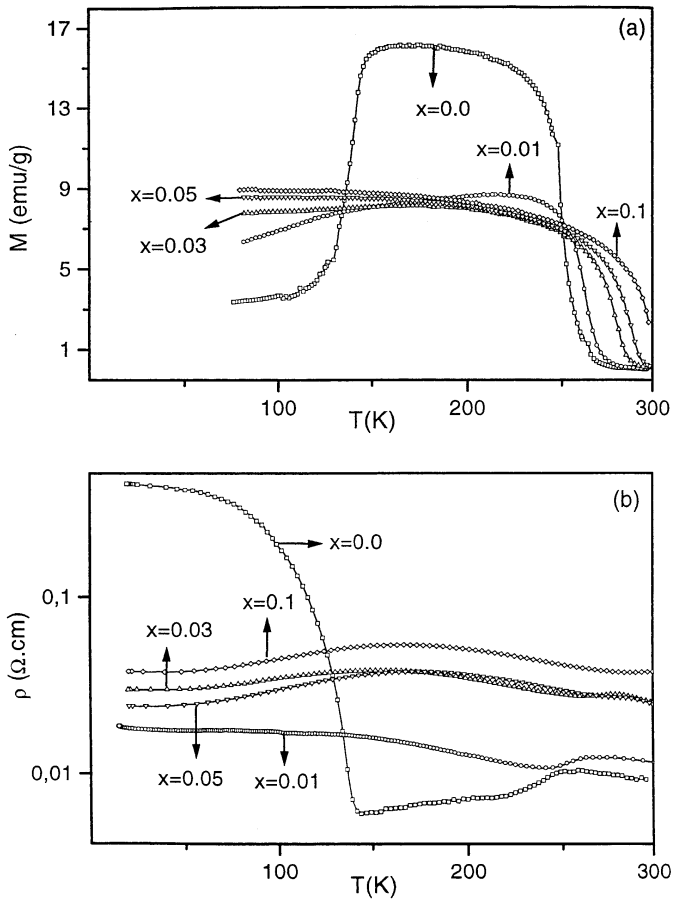

Figure 19. Temperature variation of the (a) magnetization and (b) resistivity of $Nd_{0.5}Sr_{0.5}Mn_{1-x}Ru_xO_4$ (from Vanitha *et al* [56]).

figure 21 is specially noteworthy, in that there is a reproducible memory effect in the cooling and heating cycles. The current induced I–M transition occurs even in $Y_{0.5}Ca_{0.5}MnO_3$, which is not affected by large magnetic fields. Furthermore, there is no need for prior laser irradiation to observe the current induced I–M transitions. It is proposed that electric fields cause depinning of the randomly pinned charge solid. There appears to be a threshold field in the CO regime beyond which non-linear conduction sets in along with a large broad-band conductivity noise [66]. Threshold dependent conduction disappears around T_{co} suggesting that the CO state is depinned at the onset of non-linear conduction. It is interesting that at small currents or low magnetic fields, resistance oscillations occur due to temporal fluctuations between resistive states. It is possible that inhomogeneities or phase segregation present in these materials give rise to percolative conduction [67].

9. Theoretical studies

There has been some effort to understand charge ordering in the rare earth manganates. Thus, the coupled magnetic and CO transition found at half-filling in some of the manganates has

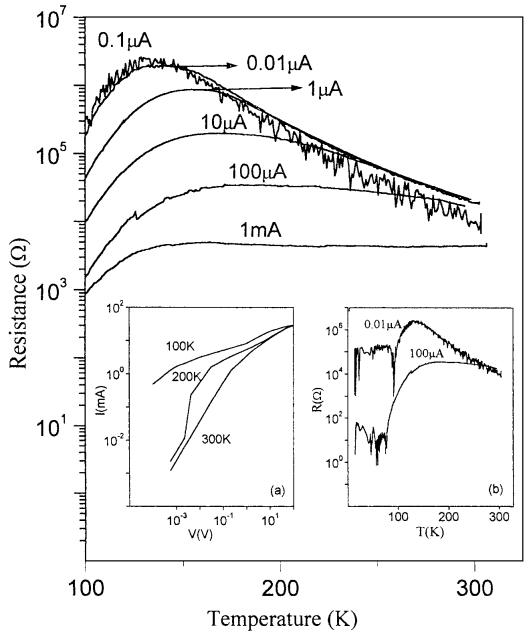

Figure 20. Electric current induced insulator–metal transition in $Pr_{0.7}Ca_{0.3}MnO_3$ films deposited on Si(100) at different values of the current. Inset (a) shows I–V curves at different temperatures. Inset (b) shows resistance oscillations at low temperatures (from Parashar *et al* [67]).

been considered to arise from an interplay between the double-exchange, superexchange and Coulomb interactions [68]. The study shows the importance of electron–electron interactions in stabilizing the CO state and predicts the occurrence of a CO–FM transition (at $x = 0.5$), coexistence of FM and AFM states as well as the effect of a magnetic field on the FM state. In the framework of dynamical mean field theory, the Holstein model for electrons interacting with phonons gives a polaronic CO state whose properties depend on the magnitude of coupling [69]. A mechanism for charge ordering in half-doped manganates has also been proposed by employing a Hamiltonian for strong Hund coupling and on-site Coulomb interactions [70]. Electron hopping results in AFM superexchange and a repulsive interaction which may drive the electrons to a Wigner lattice where the spins are aligned ferromagnetically and the localized spin background is antiferromagnetic. Based on a double exchange model which includes the coupling of electrons to Jahn–Teller distortions and finite Coulomb interaction between the e_g electrons, the FM state of $Ln_{0.5}L_{0.5}MnO_3$ is shown to be metallic and the insulating state polaronic [71]. On lowering the temperature, the FM–AFM (CE) transition occurs with a big change in resistivity. Localized $3z^2 - r^2$ polarons can give rise to the CO (CE) structure. By using the rotation-invariant local spin density approximation—U formalism, spin and orbital ordering in $Nd_{1-x}Sr_xMnO_3$ ($x = 0.5, 0.56$) has been examined [72]. While the lowest energy state is the one observed experimentally, the FM or AFM coupling between the *ab* planes is found to be sensitive to the anisotropy. There is FM coupling in the $x = 0.5$ system, and AFM coupling in the $x = 0.56$ system.

A study of the competition between long range and short range interactions among holes within a continuum formulation of the spin density waves in layered oxides has provided a charge-ordering phase diagram [73]. Long range Coulomb interaction and short range magnetic dipolar interaction are the main interactions. The different phases found include

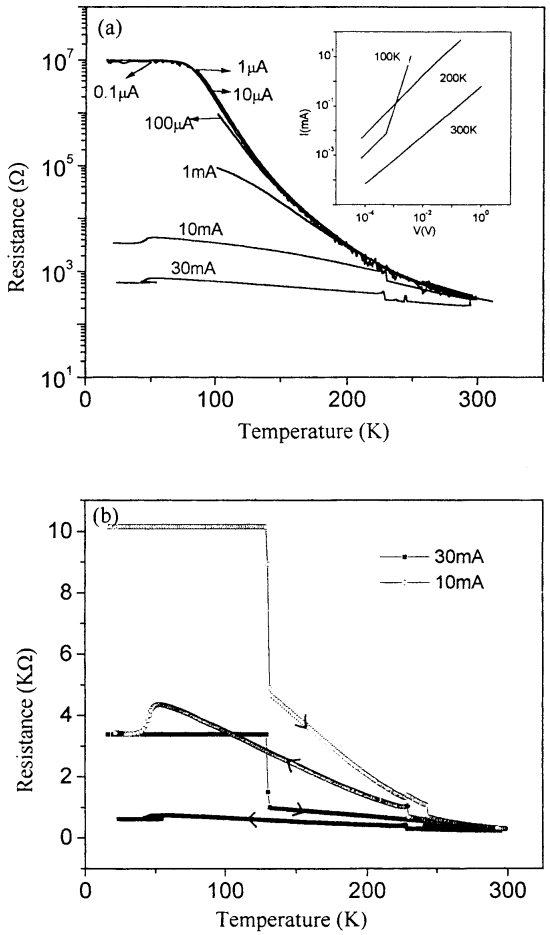

Figure 21. (a) Temperature variation of resistance of an oriented $Pr_{0.7}Ca_{0.3}MnO_3$ film deposited on $LaAlO_3(001)$ for different values of the current; (b) resistance–temperature plots for two current values recorded over cooling and heating cycles showing memory effect. Inset in (a) shows I–V curves at different temperatures (from Parashar *et al* [67]).

Wigner crystal, diagonal stripes and horizontal–vertical stripes. The extended Hubbard model with both on-site and nearest neighbour Coulomb repulsion predicts a re-entrant transition from a CO state to a homogeneous (metallic) state on cooling [74]. Such re-entrant transitions, wherein the melting of the CO state occurs on decreasing the temperature, have been observed in the manganates.

Phase separation in the manganates has been a subject of a few theoretical investigations [75, 76]. Generally, phase separation involves the formation of clusters of one phase in another (e.g. FM clusters in a CO or AFM phase). Macroscopic phase separation involving the presence of distinct domains of fairly large sizes ($\geqslant$100 nm) with Bragg peaks in the diffraction patterns is however different from the formation of clusters or stripes. Such inhomogenous distributions of CO or FM (charge and spin) phases in a material requires understanding. Coulomb forces would prevent accumulation of charge in a phase separated regime in the absence of the means to compensate the charge [76]. Such phase separation is known in $La_2NiO_{4+\delta}$ and $La_2CuO_{4+\delta}$. In the rare earth manganates, there is increasing evidence for the coexistence of FM and AFM

(CO) phases. While it is possible that small changes in the Mn^{3+}/Mn^{4+} ratio could affect phase separation [29], we are far from understanding the mechanism.

10. Concluding remarks

Charge ordering in rare earth manganates has clearly emerged to become an important area of research in condensed matter science in the last two years because of the variety of properties and phenomena exhibited by these materials and also due to the extraordinary sensitivity to various factors. The relation between orbital ordering, charge ordering and spin ordering in the rare earth manganates is of great interest. In systems such as $Pr_{0.6}Ca_{0.4}MnO_3$ and $Nd_{0.5}Ca_{0.5}MnO_3$ ($\langle r_A \rangle \approx 1.17$ Å), charge ordering occurs in a paramagnetic state (associated with FM correlations), and long range (commensurate) orbital ordering accompanies the transition to the AFM CE state. In the paramagnetic CO state, there could be some orbital ordering which would be incommensurate. In a manganate such as $Nd_{0.5}Sr_{0.5}MnO_3$ ($\langle r_A \rangle = 1.24$ Å) where charge ordering occurs on cooling an FMM state, we seem to be able to delineate transitions associated with orbital as well as charge ordering. Thus, the FM state transforms on cooling, first to an orbitally ordered AFM (A-type) state, and then to a CO AFM state (CE type) with orbital ordering. In a complex system such as $La_{0.5}Ca_{0.5}MnO_3$ ($\langle r_A \rangle = 1.20$ Å), charge ordering and orbital ordering occur when the FM state transforms to an AFM state (CE type), on cooling. In the regime where the FM and CO states co-exist, there is no long range orbital ordering. As expected, the $La_{0.5}Ca_{0.5}MnO_3$ system gives more complex lattice images. In $La_{0.33}Ca_{0.67}MnO_3$, however, there is a clear cut charge-ordering transition (260 K), accompanied by orbital ordering, followed by a transition to an AFM state (CE type). In this system, paired stripes of $Mn^{3+}O_6$ octahedra are found in the lattice images. In manganates such as $Nd_{0.5}Ca_{0.5}MnO_3$ and $Y_{0.5}Ca_{0.5}MnO_3$ with small $\langle r_A \rangle$, it is not clear whether ordered single or bi-stripes would be present. It is important to ensure that bi-stripes and other features found by electron microscopy truly represent the bulk structure. Furthermore, the nature of the lattice images corresponding to the stripes has to be fully investigated.

There are many aspects of charge ordering in the rare earth manganates that need to be further investigated. Although we can delineate spin ordering, charge ordering, and orbital ordering, some aspects are not yet fully understood. Thus, the occurrence of bi-stripes and phase separation require further study. Although one can consider the presence of large domains (e.g. CO and FM) of different phases of a given composition as a criterion for phase separation, the effects of phase separation in contrast to that of chemical inhomogeneities or cluster formation is to be understood. It is not clear whether commensurate orbital ordering occurs only in the AFM (CE) state. Charge ordering in the layered manganates has to be adequately investigated. We do not have a proper understanding of the extraordinary effect of electric fields on the CO states. The $\langle r_A \rangle$ regime of 1.20 ± 0.02 Å in $Ln_{0.5}L_{0.5}MnO_3$, exhibiting complex phenomena and properties, including re-entrant transitions, deserves greater attention. The electron–hole asymmetry in these manganates, with respect to the FM and CO states, needs to be properly explained.

Acknowledgments

The authors thank Unilever plc, University of California, Santa Barbara, and the Science Office of the European Union for support of this work.

References

[1] Valenzuela R 1994 *Magnetic Ceramics* (Cambridge: Cambridge University Press)
[2] Rao C N R, Arulraj A, Santosh P N and Cheetham A K 1998 *Chem. Mater.* **10** 2714
[3] Wollan E O and Koehler W C 1955 *Phys. Rev.* **100** 545
[4] Jirak Z, Krupicka S, Sinsa Z, Dlouha M and Vratislav S 1985 *J. Magn. Magn. Mater.* **53** 153
[5] Ramirez A P 1997 *J. Phys.: Condens. Matter* **9** 8171
Rao C N R and Raveau B (eds) 1998 *Colossal Magnetoresistance, Charge Ordering and Related Properties of Manganese Oxides* (Singapore: World Scientific).
[6] Tomioka Y, Asamitsu A, Kuwahara H, Moritomo Y and Tokura Y 1996 *Phys. Rev.* B **53** 1689
Lees M R, Barrat J, Balakrishnan G, Paul D McK and Yethiraj M 1995 *Phys. Rev.* B **52** 14 303
[7] Okimoto Y, Tomioka Y, Onose Y, Otsuka Y and Tokura Y 1999 *Phys. Rev.* B **59** 7401
[8] Tokura Y, Tomioka Y, Asamitsu A, Moritomo Y and Kasai M 1996 *J. Appl. Phys.* **79** 5288
[9] Kuwahara H and Tokura Y 1998 *Colossal Magnetoresistance, Charge Ordering and Related Properties of Manganese Oxides* ed C N R Rao and B Raveau (Singapore: World Scientific)
[10] Kawano H, Kajimoto R, Yoshizawa H, Tomioka Y, Kuwahara H and Tokura Y 1997 *Phys. Rev. Lett.* **78** 4253
[11] Goodenough J B 1955 *Phys. Rev.* **100** 564
[12] Radaelli P G, Cox D E, Marezio M and Cheong S W 1997 *Phys. Rev.* B **55** 3015
[13] Mori S, Chen C H and Cheong S W 1998 *Phys. Rev. Lett.* **81** 3972
[14] Ramirez A P, Schiffer P, Cheong S W, Chen C H, Bao W, Palstra T T M, Gammel P L, Bishop D J and Zegarski B 1996 *Phys. Rev. Lett.* **76** 3188
[15] Mori S, Chen C H and Cheong S W 1998 *Nature* **392** 473
[16] Fernandez-Diaz M T, Martinez J L, Alonso J M and Herrero E 1999 *Phys. Rev.* B **59** 1277
[17] Radaelli P G, Cox D E, Capogna L, Cheong S W and Marezio M 1999 *Phys. Rev.* B **59** 14 440
[18] Calvani P, De Marzi G, Dore P, Lupi S, Maselli P, D'Amore F, Gagliardi S and Cheong S W 1998 *Phys. Rev. Lett.* **81** 4504
[19] Kajimoto R, Kakeshita T, Oohara Y, Yoshizawa H, Tomioka Y and Tokura Y 1998 *Phys. Rev.* B **58** R11 837
[20] Mori S, Katsufuji T, Yamamoto N, Chen C H and Cheong S W 1999 *Phys. Rev.* B **59** 13 573
[21] Cox D E, Radaelli P G, Marezio M and Cheong S W 1998 *Phys. Rev.* B **57** 3305
[22] Anane A, Renard J P, Reversat L, Dupas C, Veillet P, Viret M, Pinsard L and Revcolevsci A 1999 *Phys. Rev.* B **59** 77
[23] Uehara M, Mori S, Chen C H and Cheong S W 1999 *Nature* **399** 560
[24] Kuwahara H, Tomioka Y, Asamitsu A, Moritomo Y and Tokura Y 1995 *Science* **270** 961
[25] Biswas A, Raychaudhuri A K, Mahendiran R, Guha A, Mahesh R and Rao C N R 1997 *J. Phys.: Condens. Matter* **9** L355
[26] Sekiyama A, Suga S, Fujikawa, Imada S, Iwasaki T, Matsuda K, Matsushita T, Kaznacheyev K V, Fujimori A, Kuwahara H and Tokura Y 1999 *Phys. Rev.* B **59** 15 528
[27] Biswas A, Arulraj A, Raychaudhuri A K and Rao C N R 2000 *J. Phys.: Condens. Matter* at press
[28] Mahendiran R, Ibarra M R, Maignan A, Millange F, Arulraj A, Mahesh R, Raveau B and Rao C N R 1999 *Phys. Rev. Lett.* **82** 2191
[29] Woodward P M, Cox D E, Vogt T, Rao C N R and Cheetham A K 1999 *Chem. Mater.* **11** 3528
[30] Moritomo Y, Akimoto T, Nakama A, Ohoyama K and Ohashi M 1998 *Phys. Rev.* B **58** 5544
[31] Kuwahara H, Okuda T, Tomioka Y, Asamitsu A and Tokura Y 1999 *Phys. Rev. Lett.* **82** 4316
[32] Santosh P N, Arulraj A, Vanitha P V, Singh R S, Sooryanarayana K and Rao C N R 1999 *J. Phys.: Condens. Matter* **11** L27
[33] Liu H L, Cooper S L and Cheong S W 1998 *Phys. Rev. Lett.* **81** 4684
[34] Su Y, Du C H, Hatton P D, Collins S P and Cheong S W 1999 *Phys. Rev.* B **59** 11 687
[35] Murakami Y, Shindo D, Chiba H, Kikuchi M and Syono Y 1999 *Phys. Rev.* B **59** 6395
[36] Raveau B, Maignan A, Martin C and Hervieu M 1998 *Chem. Mater.* **10** 2641
[37] Woodward P M, Vogt T, Cox D E, Arulraj A, Rao C N R, Karen P and Cheetham A K 1998 *Chem. Mater.* **10** 3652
[38] Arulraj A, Santosh P N, Gopalan R S, Guha A, Raychaudhuri A K, Kumar N and Rao C N R 1998 *J. Phys.: Condens. Matter* **10** 8497
[39] Arulraj A and Rao C N R 1999 *J. Solid State Chem.* **145** 557.
[40] Rao C N R, Santosh P N, Singh R S and Arulraj A 1998 *J. Solid State Chem.* **135** 169
[41] Moritomo Y, Kuwahara H, Tomioka Y and Tokura Y 1997 *Phys. Rev.* B **55** 7549
[42] Damay F, Martin C, Maignan A, Hervieu M, Raveau B, Jirak Z, Andre G and Bouree F 1999 *Chem. Mater.* **11** 536

[43] Lees M R, Baratt J, Balakrishnan G, Paul D McK and Ritter C 1998 *Phys. Rev.* B **58** 8694
[44] Lees M R, Petrenko O A, Balakrishnan G and Paul D McK 1999 *Phys. Rev.* B **59** 1298
[45] Rodriguez-Martinez L M and Attfield J P 1996 *Phys. Rev.* B **54** R15 622
[46] Damay F, Martin C, Maignan A and Raveau B 1997 *J. Appl. Phys.* **82** 6181
[47] Attfield J P 1998 *Chem. Mater.* **10** 3239
[48] Vanitha P V, Santosh P N, Singh R S, Rao C N R and Attfield J P 1999 *Phys. Rev.* B **59** 13 539
[49] Tokura Y, Kuwahara H, Moritomo Y, Tomioka Y and Asamitsu A 1996 *Phys. Rev. Lett.* **76** 3184
[50] Arulraj A, Biswas A, Raychaudhuri A K, Rao C N R, Woodward P M, Vogt T, Cox D E and Cheetham A K 1998 *Phys. Rev.* B **57** R8115
[51] Ishikawa T, Ookura K and Tokura Y 1999 *Phys. Rev.* B **59** 8367
[52] Tokunaga M, Miura N, Moritomo Y and Tokura Y 1999 *Phys. Rev.* B **59** 11 151
[53] Hess C, Büchner B, Hücker M, Gross R and Cheong S W 1999 *Phys. Rev.* B **59** R10 397
[54] Li J Q, Matsui Y, Kimura T and Tokura Y 1998 *Phys. Rev.* B **57** 3205
[55] Argyriou D N, Bordallo H N, Cambell B J, Cheetham A K, Cox D E, Gardner J S, Hanif K, dosSantos A and Strouse G F at press
[56] Vanitha P V, Singh R S, Natarajan S and Rao C N R 1999 *Solid State Commun.* **109** 135
Vanitha P V, Arulraj A, Raju A R and Rao C N R 1999 *C. R. Acad. Sci. Paris* to be published
[57] Barnabe A, Hervieu M, Martin C, Maignan A and Raveau B 1998 *J. Mater. Chem.* **8** 1405
[58] Babushkina N A, Belova L M, Gorbenko O Yu, Kaul A R, Bosak A A, Ozhogin V I and Kugel K I 1998 *Nature* **391** 159
[59] Zhao G, Ghosh K, Keller H and Greene R L 1999 *Phys. Rev.* B **59** 81
[60] Garcia-Landa B, Ibarra M R, De Teresa J M, Zhao G, Conder K and Keller H 1998 *Solid State Commun.* **105** 567
[61] Mahesh R and Itoh M 1999 *J. Solid State Chem.* **144** 232
[62] Miyano K, Tomaka T, Tomioka Y and Tokura Y 1997 *Phys. Rev. Lett.* **78** 4257
[63] Feibig M, Miyano K, Tomioka Y and Tokura Y 1998 *Science* **280** 1925
[64] Kiryukhin V, Wang Y J, Chou F C, Kastner M A and Birgeneau R J 1999 *Phys. Rev.* B **59** R6581
[65] Ponnambalam V, Parashar S, Raju A R and Rao C N R 1999 *Appl. Phys. Lett.* **74** 206
[66] Guha A, Ghosh A, Raychoudhuri A K, Parashar S, Raju A R and Rao C N R 1999 *Appl. Phys. Lett.* **75** 3381
[67] Parashar S, Ebenso E E, Raju A R and Rao C N R 1999 to be published
[68] Babushkina N A, Belova L M, Khomskii D I, Kugel K I, Gorbenko O Yu and Kaul A R 1999 *Phys. Rev.* B **59** 6994
[69] Mishra S K, Pandit R and Satpathy S 1998 *J. Phys.: Condens. Matter* **43** 8561
[70] Ciuchi S and de Pasquale F 1999 *Phys. Rev.* B **59** 5431
[71] Shen S Q and Wang Z D 1999 *Phys. Rev.* B **59** 14 484
[72] van Veenendaal M and Fedro A J 1999 *Phys. Rev.* B **59** 15 056
[73] Fujiwara T and Korotin M 1999 *Phys. Rev.* B **59** 9903
[74] Stojkovic B P, Yu Z G, Bishop A R, Castro Neto A H and Gronbech-Jensen N 1999 *Phys. Rev. Lett.* **82** 4679
[75] Peitig R, Bulla R and Blawid S 1999 *Phys. Rev. Lett.* **82** 4046
[76] Riera J, Hallberg K and Dagotto E 1997 *Phys. Rev. Lett.* **79** 713
[77] Yunoki S, Hu J, Malvezzi A L, Moreo A, Furukova N and Dagotto E 1998 *Phys. Rev. Lett.* **80** 845